

Supplementary Information:

Imaging stray magnetic field of individual ferromagnetic nanotubes

D. Vasyukov^{1,#}, L. Ceccarelli^{1,#}, M. Wyss¹, B. Gross¹, A. Schwab¹, A. Mehlin¹, N. Rossi¹, G. Tütüncüoglu², F. Heimbach³, R. R. Zamani⁴, A. Kovács⁵, A. Fontcuberta i Morral², D. Grundler⁶, and M. Poggio¹

¹ Department of Physics, University of Basel, 4056 Basel, Switzerland

² Laboratory of Semiconductor Materials, Institute of Materials (IMX), School of Engineering, École Polytechnique Fédérale de Lausanne (EPFL), 1015 Lausanne, Switzerland

³ Lehrstuhl für Physik funktionaler Schichtsysteme, Physik Department E10, Technische Universität München, 85747 Garching, Germany

⁴ Solid State Physics, Lund University, 22100 Lund, Sweden

⁵ Ernst Ruska-Centre for Microscopy and Spectroscopy with Electrons, Forschungszentrum Jülich, 52425 Jülich, Germany

⁶ Laboratory of Nanoscale Magnetic Materials and Magnonics, Institute of Materials (IMX), School of Engineering, École Polytechnique Fédérale de Lausanne (EPFL), 1015 Lausanne, Switzerland

Contributed equally.

E-mail: martino.poggio@unibas.ch

Approach and navigation

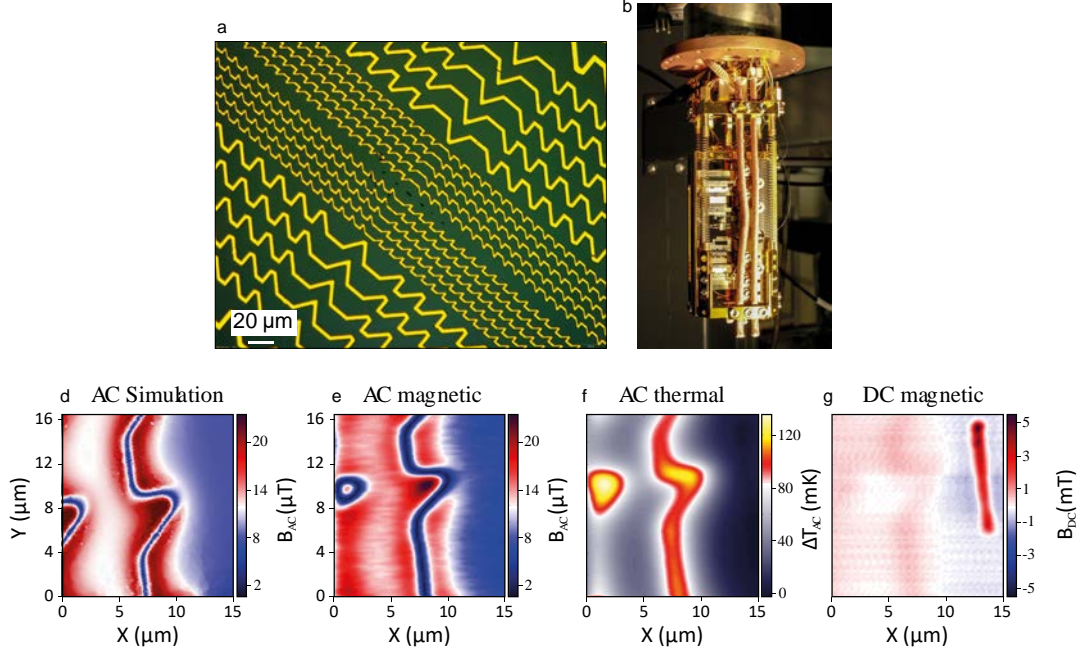


Fig. S1. (a) Optical image of the sample showing the patterned continuous Au wire for navigation and FNTs (dark lines in the middle); (b) photograph of the SOT microscope; (d) simulation of the AC magnetic field amplitude along the z-axis B_{AC} produced by the current flowing through the Au wire; corresponding measurements of (e) B_{AC} , (f) the thermal signal ΔT_{AC} , and (g) the DC magnetic field along the z-axis B_{DC} , recorded by the SOT above the area with ferromagnetic nanotube (visible in DC magnetic image).

The nanotube samples under study lie on a substrate and are difficult to locate with a scanning probe. Typically, such problems are solved by using topographic markers to locate the samples. Our scanning probe is not sensitive to sample topography and the use of magnetic markers could cause unwanted interactions with the ferromagnetic nanotubes (FNTs). Fortunately, the SOT devices are extremely sensitive to the AC magnetic field [27] and heat [40], which can both be used for navigation. We therefore pattern a continuous Au wire on our sample substrate. By passing an AC current through the wire, we can image its geometry and use it as a marker of position. In fact, the wire serves two purposes: 1) we use it to locate the nanotubes and navigate above them at a safe distance $>1 \mu\text{m}$; 2) by comparing the measured AC magnetic field produced by the wire with simulations of the Biot-Savart field, we use the wire to determine the distance between the substrate and the SOT. Once navigation is complete and the distance has been determined, we can turn the AC current off removing any disturbance to the measurements of the FNT magnetism. The asymmetric structure of the wire and its varying period create a “hot” area in the middle of the sample, which is used for rough navigation a few hundred μm above. Upon approach the wire features become visible in the magnetic and thermal signals. Thereafter, finding the location of the nanotube is easy.

Image processing

Imaging with nanoSQUIDs provides a spatial resolution, which is limited by the finite size of the sensor and the sample-to-sensor separation. If the diameter of the SQUID pick-up loop is bigger than this separation, it makes sense to consider the size and shape of the SQUID loop in deconvolving the measured flux image to extract an image of the stray field. All the images shown in this work were processed with a filter function. Using the convolution theorem we assume that our data matrix in the 2D Fourier space is represented by:

$$b_r(k_x, k_y, z) = b_f(k_x, k_y, z) \cdot g(k_x, k_y)$$

Where b_r is the 2D Fourier transform of the raw data matrix, b_f is the filtered data matrix in Fourier space and g is the filter function. Additionally k_x and k_y are components of the spatial frequencies, while z is assumed constant, playing the role of multiplicative factor (the height of the SQUID over the sample is considered constant since the tilt of the sample is negligible). As a filter function we used a Boolean matrix in the real space, with the same number of elements as in the data matrix. It has the same geometrical characteristics and dimensions as the SOT probe.

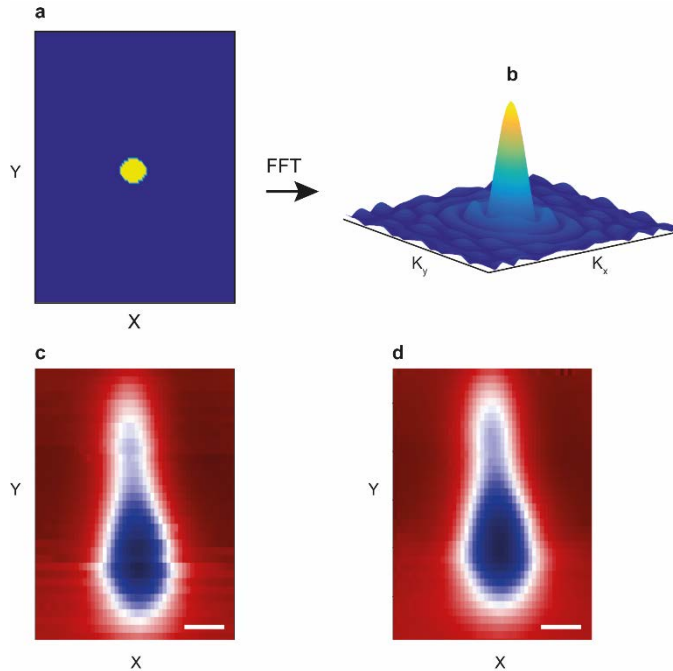


Fig. S2. Images of (a) $G(x, y)$ function, (b) $g(k_x, k_y)$ function, (c) raw flux image of a nanotube, (d) stray field of a nanotube (deconvolved). Scale bar is $0.7 \mu\text{m}$ and the signal span is 15 Gauss.

The function in real space on the right is described by:

$$G(x, y)|_{z=cost.} = \begin{cases} 1, & |r| < a \\ 0, & |r| \geq a \end{cases}$$

Where a stands for the radius of the SQUID loop. Then G is the filter function in the real space. Applying a 2D Fourier transform was obtained a first order Bessel function in the Fourier space:

$$g(k_x, k_y) = \iint G(x, y) e^{-j2\pi(xk_x + yk_y)} dx dy \propto J_1(k_x, k_y)$$

The same procedure, i.e. a 2D Fourier transform was applied to the raw data to obtain the b_r matrix, after which the b_f function can be extracted by multiplying the b_r and g^{-1} :

$$b_f(k_x, k_y, z) = b_r(k_x, k_y, z) g^{-1}(k_x, k_y)$$

The filtered real space matrix was obtained by the Fourier transform inversion of the b_f function.

We note that this filtering procedure does not significantly alter the images, reflecting the small size of the SOT probe compared to the length-scales over which our measured stray field vary. Figure S2 demonstrates the images before and after the applied deconvolution.

Stray-field images of 2-μm-long FNT

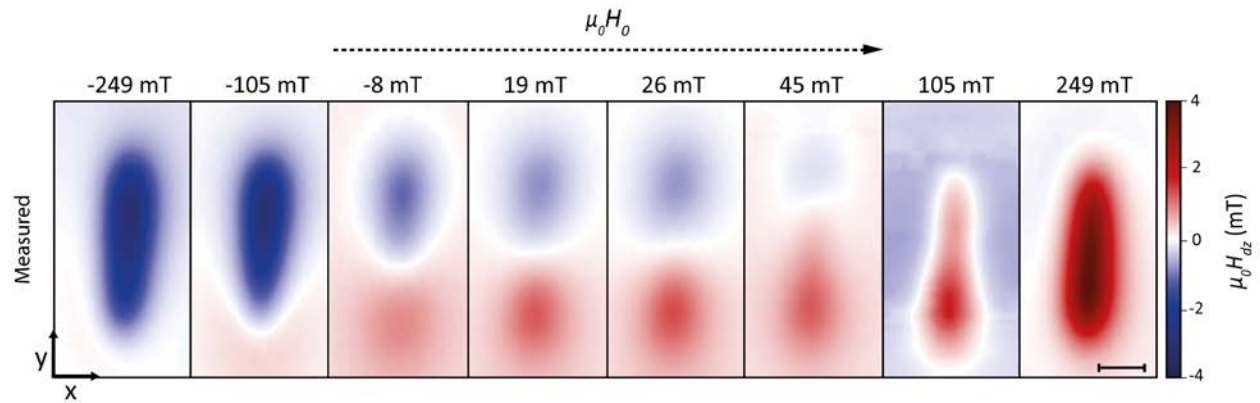


Fig. S3. Magnetic reversal of a 2-μm-long FNT ($l = 2.06 \mu\text{m}$, $d = 230 \text{ nm}$) in a field H_0 applied perpendicular to its long axis. Images of the stray field component along \hat{z} , H_{dz} , in the xy -plane 300 nm above the FNT for the labeled values of H_0 as measured by the scanning SOT. The scalebar corresponds to 1-μm. This FNT displays a qualitatively similar reversal progression to the 4-μm-long FNT in Fig. 2 of the text.

Setting the initial conditions of the simulation

The simulated stray field pattern near $H_0 = 0$ for the 0.7- μm -long FNT (Figs. 3 (b) and 3 (c)) depends on the initial conditions of the simulation. For this reason, a number initial conditions were tested.

In the simplest case, shown in Fig. 3 (c), the FNT was initialized at $H_0 = 0$ with a vortex at each end of matching circulation sense and an axial central domain. In the simulation, this mixed state configuration is then allowed to relax to a stable low energy configuration at $H_0 = 0$. The resulting zero-field configuration is the slightly distorted global vortex state shown in the middle panel of Fig. 3 (d). The field is subsequently stepped to -45 mT in small steps, always allowing the system to find a stable low energy configuration at each field. This procedure preserves the global vortex state down to -45 mT, which is the starting point for the stray field simulation shown in Fig. 3 (c). At this point, the field is stepped up towards 57 mT. Again, at each field the system is allowed to find a stable low energy configuration.

For the progression shown in Fig. 3 (b), the FNT is initialized with two vortices, one each in the top and bottom facets of the hexagonal FNT. This configuration is initialized at $H_0 = 0$ and allowed to relax. Then, once again, the magnetic field is stepped to -45 mT, always allowing the system to find a stable low energy configuration. At this point, as before, the field is stepped up towards 57 mT.

A number of other initial configurations were tested, including with up to 6 vortices in various positions in the FNT. We also initialized the simulation with a saturated FNT by applying a strong field $H_0 < -1.2$ T and stepping the field back towards the starting point at -45 mT. None of these procedures produced the stray-field patterns that we observed in Fig. 3 (a). It is impossible for us to rule out that other stable magnetization configurations – different than those we suggest – produce the observed stray field patterns. Nevertheless, having tested the most probable configurations according to both theoretical predictions and previous experiments, the predicted configurations are likely close to reality.